REPORT DOCUMENTATION PAGE

Form Approved OMB No. 0704-0188

1. REPORT DATE *(DD-MM-YYYY)*	2. REPORT TYPE	3. DATES COVERED *(From – To)*
05-08-2004	Final Report	24 April 2003 - 24-Apr-04

4. TITLE AND SUBTITLE

Experimental Study of Josephson Qubits and Oscillators

5a. CONTRACT NUMBER
FA8655-03-1-3037

5b. GRANT NUMBER

5c. PROGRAM ELEMENT NUMBER

6. AUTHOR(S)

Professor Alexey V Ustinov

5d. PROJECT NUMBER

5d. TASK NUMBER

5e. WORK UNIT NUMBER

7. PERFORMING ORGANIZATION NAME(S) AND ADDRESS(ES)

University of Erlangen-Nuremberg
Erwin-Rommel-Str. 1
Erlangen 91058
Germany

8. PERFORMING ORGANIZATION REPORT NUMBER

N/A

9. SPONSORING/MONITORING AGENCY NAME(S) AND ADDRESS(ES)

EOARD
PSC 802 BOX 14
FPO 09499-0014

10. SPONSOR/MONITOR'S ACRONYM(S)

11. SPONSOR/MONITOR'S REPORT NUMBER(S)
SPC 03-3037

12. DISTRIBUTION/AVAILABILITY STATEMENT

Approved for public release; distribution is unlimited.

13. SUPPLEMENTARY NOTES

14. ABSTRACT

This report results from a contract tasking University of Erlangen-Nuremberg as follows: The Grantee will investigate physical properties and improve the performance of two groups of Josephson devices: Josephson junction array oscillators and Josephson Qubits. They will continue study of series-parallel Josephson junction array oscillators from earlier research. The goal is to significantly increase the detected radiated power from 80 GHz to 120 GHz by improving the resonance frequency match between the devices and the receiver. They will also test the compact arrays of similar oscillator devices which incorporate antenna wires. Second, they will design and fabricate Josephson qubit devices for characterization from 4.2 K down to 20 mK. The energy profile will be characterized in the classical regime and projected into the quantum range and the coupling of the qubits to the environment will be examined according to the approach detailed in the technical proposal.

15. SUBJECT TERMS
EOARD, Quantum Bits, Qbits, Josephson junctions, Qubits

16. SECURITY CLASSIFICATION OF:			17. LIMITATION OF ABSTRACT	18, NUMBER OF PAGES	19a. NAME OF RESPONSIBLE PERSON
a. REPORT	b. ABSTRACT	c. THIS PAGE			/Signed/PAUL LOSIEWICZ, Ph. D.
UNCLAS	UNCLAS	UNCLAS	UL		19b. TELEPHONE NUMBER *(Include area code)* +44 20 7514 4474

Final Report (No.3)

Experimental study of Josephson qubits and oscillators*

J. Lisenfeld, A. A. Abdumalikov and A. V. Ustinov

Physikalisches Institut III, Universität Erlangen-Nürnberg
D-91058 Erlangen, Germany

* Supported by European Office of Aerospace Research and Development (EOARD)
under Contract FA8655-03-1-3037

July 2004

Contents

Abstract

This final report summarizes our activities and results obtained within the three sub-projects of the founded research.

The first part focusses on measurements in the quantum regime at millikelvin temperatures. New designs of quantum bits made from single current-biased Josephson junctions are evaluated regarding their usability for quantum computation, which is generally limited by decoherence effects. Our intention was to limit decoherence by decoupling the junction via microwave engineered planar circuits. This new approach has been evaluated for our sample designs using spectroscopical measurements of the coherence time. We also report about achievements in our experimental technique to measure and control the qubit quantum state in the time domain.

The second sub-project deals with the study of a persistent supercurrent multi-Josephson junction qubit whose circuit is based on flattened Josephson junction triangular prism. The qubit have been designed and fabricated using Nb-AlO_x-Nb technology. Measurement results at 4.2 K are presented. The state of a qubit has been detected by a dc-SQUID. We observe clear signatures of coupling between the read-out SQUID and the qubit. The SQUID response has a hysteresis related to different states of the qubit.

Thirdly, we report on radiation measurements from a series-parallel array (SPA). The measured arrays have shown three resonant steps on their current-voltage characteristics at different frustrations. We have detected radiation from all three resonances, where the largest detected power was about 14 pW.

1 Low temperature experiments on Josephson junction qubits

1.1 Introduction

Josephson junctions are key ingredients to nearly all designs of superconducting quantum bits. The most fundamental type of a qubit is represented by a single current biased junction. The quantum mechanical properties of the junction can be described using only the macroscopic phase difference φ of the Cooper pair condensates across the junction. These macroscopic quantum properties can be observed when the junction is cooled below a typical cross-over temperature of about 100 mK, where thermal fluctuations are small compared to the difference in energy between the discrete energy levels, see Fig. 1. The positions of these levels and the potential barrier height U_0 can be controlled through the applied bias current.

Quantum tunnelling through the potential barrier is associated with an onset of a small DC voltage across the junction, and this allows to directly observe each tunnelling event. The measured tunnelling probability contains information about the population of the discrete levels. Transitions between levels and thus a control of the quantum state can be realized by applying microwave pulses, tuned in resonance with the energy level spacing.

When the junction is used as a quantum bit, its two lowest levels are chosen as the logical basis states $|0\rangle$ and $|1\rangle$ in which quantum information will be encoded. Logical operations and a state readout is performed via sequences of short microwave and DC pulses.

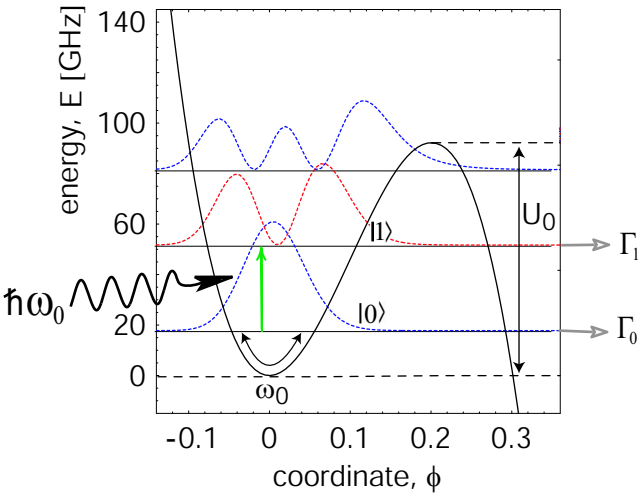

Figure 1: Potential encountered by the phase difference ϕ of a single Josephson junction. Microwaves at photon energies equal to the level spacing induce transitions between quantum states, from which quantum tunnelling through the barrier occurs at a rate Γ.

Decoherence is the crucial problem for superconducting qubits, since it limits the life time of quantum information. Apart from current noise reaching the sample through the biasing wires, the coupling of the qubit to its electromagnetic environment is a major source for the decoherence. Properly isolating the junction from its environment is therefore a vital point in this research. Recent encouraging experiments showed [1] that by careful sample design, the coherence time could be made long enough (up to $1\,\mu$s) to observe Rabi oscillations and demonstrate NMR-like quantum state control by applying sequence of microwave pulses.

In Erlangen, we have two He^3/He^4 dilution cryostats available to perform experiments in the quantum regime at temperatures down to 20 mK. The technique to characterize the samples is well-established in our laboratory. Using a current-ramp setup [2], we detect resonant photon-absorption processes in an applied microwave field. We can spectroscopically determine both the positions and widths of the energy levels, where the latter provide a direct measure of the quality factor of the quantum bit.

The basic observable in our experiments is the tunnelling-escape rate Γ. It depends exponentially on bias current and drops below few Hz at bias currents below 96% of the critical current. Escape from the first excited level is typically 1000 times more probable than from the ground state, and so an enhancement in the escape rate indicates a population in excited states.

1.2 Reducing decoherence

The crucial factor deciding about the useability of a quantum bit is its coherence time, which can be described as the duration for which the qubit's quantum state does not decay due to environmental interactions. Current fluctuations in the junction bias are the major external source for decoherence in the discussed type of quantum bit. Noise currents at low frequencies will vary the energy level separation, while noise at frequencies comparable to the level separation will induce unwanted transitions between levels. The junction's quality factor (Q-factor) is a measure for coherence and equals the number of plasma oscillations the qubit can undergo within the decoherence time. The declared lower limit for successful quantum information processing is a Q-factor of 10^4 [3].

Figure 2 shows measured data of a small Josephson junction with an area of 10 μm^2, taken at a temperature of 20 mK. The left plot shows rate enhancement curves for resonant photon absorption for two different frequencies. We define the rate enhancement Γ^* as the ratio of the escape rate with applied microwave Γ to the rate without applied microwave Γ_0: $\Gamma^* = \frac{\Gamma - \Gamma_0}{\Gamma_0}$. A Lorenzian peak (resonance) occurs in the rate enhancement, when the externally applied microwave equals the frequency associated with the energy level separation, .

The quality factor is given by the formula

$$Q = \frac{f}{\Delta f},$$

where Δf is the width of the peak and f is the applied microwave frequency. In the data of Fig. 2 (a), the Lorenzian peaks have a width $\Delta f \approx 80$ MHz at a frequency of 15.9 GHz, from which we calculate a quality factor of $Q \approx 200$.

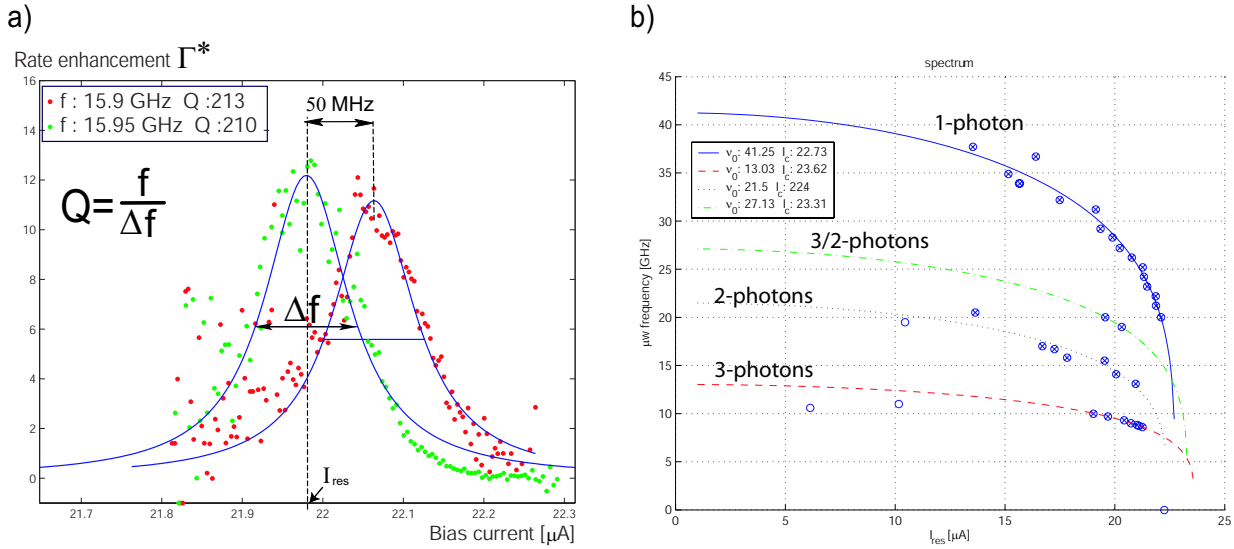

Figure 2: (a) Lorenzian peak in the tunnelling rate indicating resonant microwave photon absorption. The spectroscopic quality factor Q at the qubit transition frequency f is calculated from the peak width Δf. (b) Measured energy spectrum of the quantum bit (dots) and fits to theory (lines). The dots mark the bias-currents $I_{\rm res}$ of detected microwave resonance peaks at their corresponding frequency.

To obtain the energy spectrum of the qubit, we search a large frequency range for resonant photon absorption peaks in the escape rate. The bias current positions of their maxima is then plotted versus the corresponding frequency, as it is shown for the same junction in Fig.

2 (b). The solid line shows the fitted theoretical dependence of the energy level separation $\nu(I)$ versus bias current I, as it is given by the formula

$$\nu(I) = \nu_0 \left[1 - \left(\frac{I}{I_c}\right)^2\right]^{1/4}. \quad (1)$$

Here ν_0 is the zero-bias plasma frequency of the junction and I_c is its critical current. The figure shows that most of the found resonances obey this relation, while others can be fitted to integer fractions of Eq. (1) (dashed lines). This is explained by multi-photon absorption, where an integer number of photons is absorbed at the same time. For this kind of process, the energy difference between the levels is equal to n times the photon energy, where n is an integer number. The resonance of 3/2 photons can be interpreted as a transition to the second excited state by absorption of three photons.

Decoupling by microwave circuits. Since the plasma frequency of Josephson junctions is in the microwave range from 10 to 40 GHz, it is important to have a well-designed electromagnetic environment for the qubit at these frequencies. In particular, the environment impedance must be made as large as possible to prevent coupling to the low-impedance junction. It has been shown [1] that broadband impedance transformers can substantially increase the quality factor of small junctions. We have chosen an approach to embed the quantum bit in a superconducting planar microwave circuit, see Fig. 3.

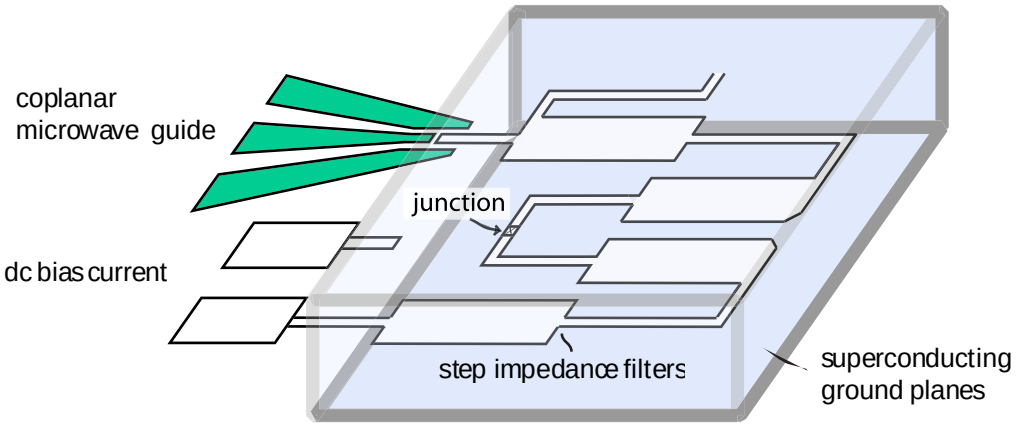

Figure 3: Sketch of the on-chip microwave design, not drawn to scale for better visibility.

Samples which were tested in our lab feature on-chip microwave filters in a stripline-architecture and coplanar waveguides to inject high frequency currents [4]. Both the filters and the junction are placed between two superconducting ground planes which are supposed to reduce radiation losses as well as dielectric losses in the substrate. Each filter consists of several stripline segments where low impedance sections (broad lines) are followed by high impedance sections (narrow lines), each as long as half the wavelength of the junction plasma oscillations. We optimized the designs with the aid of computer simulations to exhibit the required microwave characteristics, which are a large attenuation at the qubit transition frequency and a low admittance at the place of the junction. The latter is crucial since the real part of the environmental admittance shunting the junction contributes to dissipation and thus lowers the Q factor.

Results. Fig. 4 (a) shows a result of the simulations which were done in the process of designing the microwave stripline filter. It plots the transmission of microwave power from the coplanar waveguide to the junction. The goal here was to have a large attenuation (more than 40 dB) in a broad range around the desired qubit transition frequency of 16 GHz,

to effectively shield the junction from high frequency current noise. In addition, in order to control the quantum state, it is necessary to apply a microwave current to the junction exactly at the transition frequency. To make the stripline filter transparent only for this frequency, we created a resonator inside the filter box. Fig. 4 (a) shows that the characteristics of the filter including the resonator exhibits a peak in transmission at the resonator's frequency of 16 GHz.

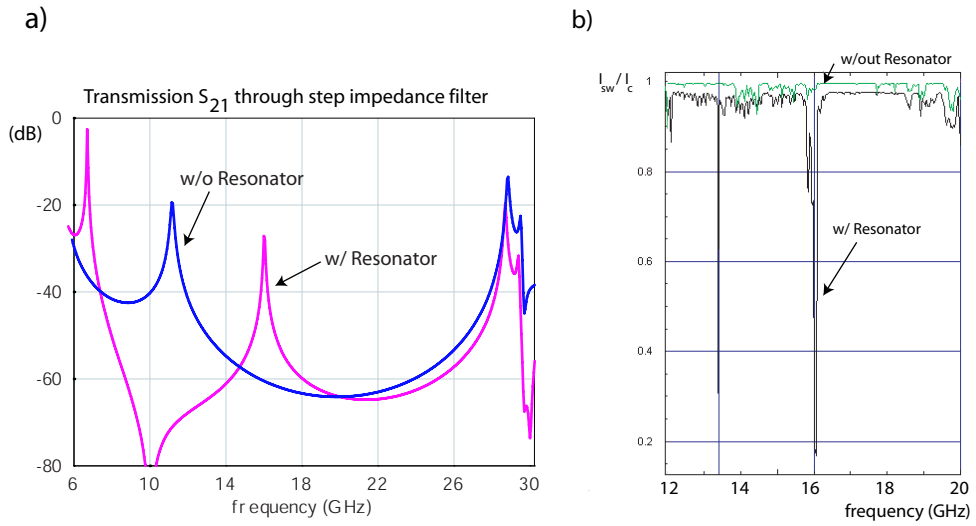

Figure 4: (a) Simulation of the structure of Fig. 3, showing the transmission from the coplanar waveguide to the junction inside the step impedance filter. (b) Measured switching current dependence of the qubit versus applied microwave frequency for a large-amplitude signal. The dark line shows a resonance at 16 GHz which is due to the additional resonator in the design. An additional spurious resonance of unknown origin can be seen at 13.4 GHz. The light curve was measured at an identical sample which did not include the resonator.

Experimentally, we verified that the designed filter is working as expected by using the fact that the critical current of a Josephson junction will be strongly suppressed if it is irradiated at high microwave powers. By applying a large-amplitude microwave signal and varying its frequency while continuously monitoring the critical current of the junction, we have measured how much of the signal passes through the filter to the junction. The result of this measurement is plotted in Fig. 4 (b) for two different samples: one which has a resonator tuned to 16 GHz and one without a resonator. We find that the sample with the embedded resonator indeed shows a sharp suppression of the critical current at the resonance frequency, while for the sample without a resonator this feature does not exist. For both samples, the critical current could be suppressed also with relatively low microwave powers when the frequency was chosen to lie outside the working cut-off band of the filter, i.e. below about 6 GHz and above 28 GHz.

Connecting a resonator to the junction was furthermore motivated by a theoretical paper [5] which proposed that the intrinsic Q-factor of the qubit can be increased by coupling it to a resonator. Our experiments with different samples containing resonators at several resonance frequencies however did not show improvements to the coherence times. In contrast, we observed that these junctions were of even lower Q than those without filters and resonators. We suppose that there might be several reasons for this behavior:

- The superconducting ground planes of the stripline filters which surround the junction are very likely to trap magnetic flux when the sample is cooled down. This leads to vortices of circulating currents in the ground planes, which generate a local magnetic field.

Experimentally, we observed that the critical current of a junction will be substantially suppressed by these magnetic fields. Moreover, we experienced sudden changes in the critical current of the junction when an applied microwave exceeded a certain threshold power. We explain this by a vortex which changes its position, being pushed by microwave among different pinning centers. When the junction was removed or connected to the measurement electronics, flux trapping occurred more frequently than in junctions which were not embedded in stripline filters. To remove the flux, it is necessary to heat the sample above the critical temperature of niobium and cool down again, which is a time-consuming process and therefore very inconvenient.

- In spite of the fact that the stripline filters are working as expected, we believe they did not increase the coherence times because the relevant noise is not of high frequency where the filter is working, but of low frequency. This is supported by the fact that we could actually increase the Q-factors of our qubit samples from 40 to 200 by installing current dividers in the dc-bias wires. These devices work by directing most of the applied current through a low-value shunting resistor, while only a small fraction flows through the junction which is connected via a large resistance. The signal-to-noise ratio is thus effectively increased.

1.3 Implementation of time-domain measurements

In a switching current measurement, the bias current is swept linearly in time to record a switching current histogram, from which the escape rate can be easily extracted. Although this kind of measurement technique provides for fast determination of the sample parameters like critical current and plasma frequency, a different approach using stable biasing at a constant current close to the critical current is necessary to control the quantum state and to measure the escape rate in the time domain.

Results

Quantum-state control. Instrumental facilities for quantum-state control have now been implemented in our laboratory. We are able to monitor the tunnelling rate in the time domain when a constant bias current is applied to the sample. The exponential decay law for the ground state with its lifetime being limited by quantum tunnelling to the voltage state of the junction, can be observed by recording the statistical distribution of the switching times t_{esc}. For N=10000 times, we trigger a time interval counter of picosecond resolution by the pulses switching on the current source and an escape event signal from the qubit.

We observe exponential decay from the ground and excited levels, at a resolution of about 15 nanoseconds. Moreover, we accomplished and already tested the application of arbitrary sequences of microwave and DC pulses of nanosecond widths to the qubit. For this, we use a two-channel, programmable Agilent E81130A pulse generator to synchronize the time measurement with bias current and microwave pulse control. Its secondary output channel is used to generate DC pulses at a minimum width of 750 ps. The microwave source generates pulses up to 40 GHz of widths of 20 ns, which are combined by a directional coupler with the DC pulses and sent through a coaxial line to the sample. This technique opens now for us the door to coherent manipulation of the quantum state and monitoring its evolution.

State readout. Furthermore, we implemented and tested a quantum state readout scheme which involves the use of a short DC pulse. During the pulse, the tunnel rate is exponentially increased such that a larger number of tunnelling events can be registered, each with a probability P_{esc} proportional to the population of the excited state. Use of a readout

pulse also increases the instrumental resolution of the time measurement which is then limited only by the readout pulse duration.

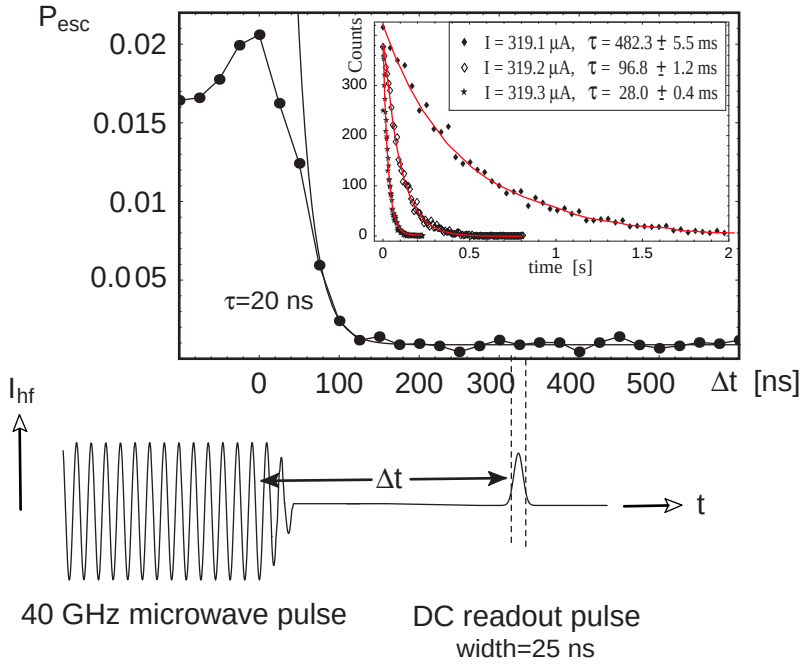

Figure 5: Results of an experiment to measure the decay from an excited state which is populated by a microwave pulse at 40 GHz frequency. A DC readout pulse has been added to the high frequency component $I_{\rm hf}$(t) of the bias current to probe the excited level population at the time Δt after the microwave pulse was switched off. Inset: A direct observation of the tunnelling probability from the ground state versus time showing exponential decay.

Figure 5 shows how a DC pulse is used to measure the dissipation-induced decay from the excited level. The readout pulse delay Δt relative to the end of the microwave pulse, which induces resonant transitions to the excited level, is hereby varied. We observe an exponential decrease of P_{esc} when Δt is increased, as expected.

With this technique it is in principle possible to observe coherent (Rabi) oscillations and to measure directly the relaxation and dephasing rates of our qubits. Standard techniques as known from NMR like spin-echo and Ramsey-fringes can be implemented to measure and reduce the effect of low-frequency noise.

Faster measurement. A major problem in the above kind of experiment was an exponential growth of the lifetime and hence the required measurement time when the bias current was decreased. This problem could be solved by switching off the bias current after the time $t_{stop} \approx 4$ ms and sending a stop event pulse to the counter.

Data evaluation is performed in a two-fold way: if more than 75% of the events are registered at times before t_{stop}, a histogram can be generated from the data and the escape rate is found with an accuracy of 1% from an exponential fit. In Fig. 6, the time-dependence of the bias current is shown together with a measured histogram, reflecting the escape probability versus time.

The events of no-tunnelling before the stop pulse will accumulate in a sharp peak of the counts at t_{stop} . We note the number of events N_{esc} registered before the stop time, related to the total number N of measurements, the escape probability: $P_{esc} = \frac{N_{esc}}{N}$. This value can

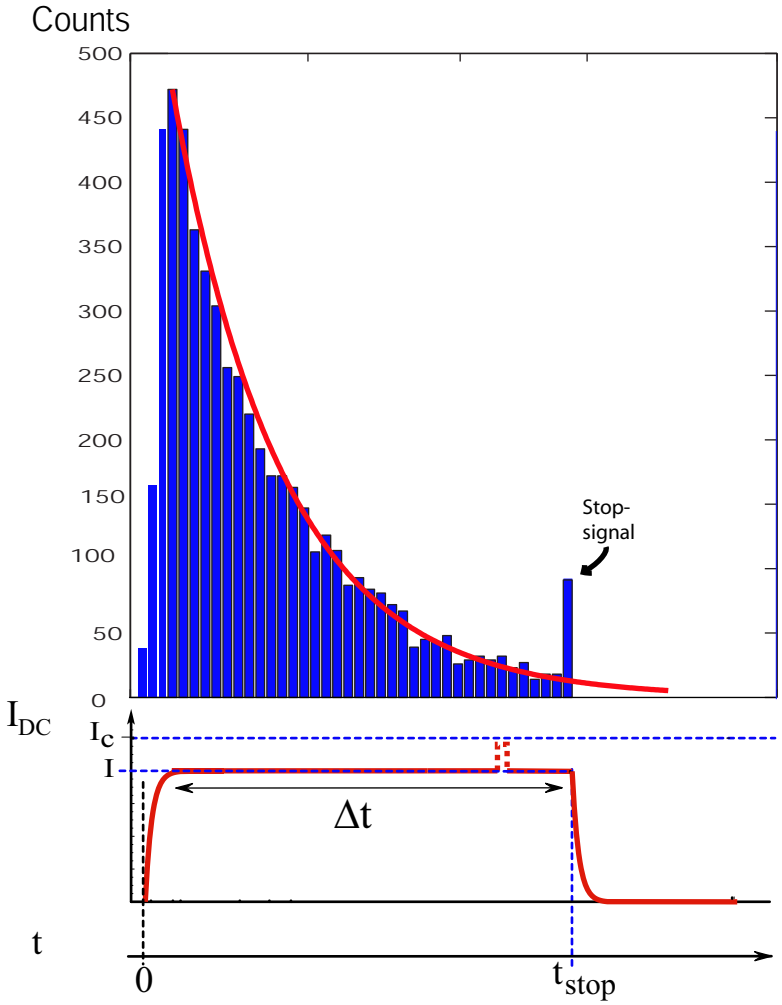

Figure 6: Upper part: typical histogram of escape events displaying the number of counts per bin versus time. An exponential fit to its envelope (red line) gives an accurate estimation of the escape rate. Lower part: time dependence of applied bias current. The dashed peak on I_{DC} represents an optional readout pulse.

be calculated by the formula

$$P_{esc} = 1 - \exp\left(-\Gamma \cdot t_{stop}\right) \tag{2}$$

and, accordingly, the escape rate Γ can be extracted from the measured P_{esc}. We found that this procedure gives a good estimation for the case when the escape rate is lower than $\approx 1/t_{stop} = 250$ Hz. The results for the escape rates obtained with and without use of the stop pulse are compared in Fig. 7. Repeating the measurement 10.000 times at a rate of 200 Hz and setting Δt to 4 ms, results in a measurement time of 50 s for one value of bias current. This is considerably faster than our former procedure (without using a stop pulse and always waiting for the junction escape), where one measurement takes an average of 6 minutes. This improvement is relevant because, for most experiments, we need to sweep more than one variable (for example, bias current and microwave power), resulting in usually from 400 up to 1000 of histograms needed to be acquired. The estimated lower limit of the measurable escape rate with this new procedure is about 1 Hz.

The upper limit of measurable escape rates is hereby determined by the bandwidth of the bias current lines, because it limits the rise time of the current. For high bias currents, due

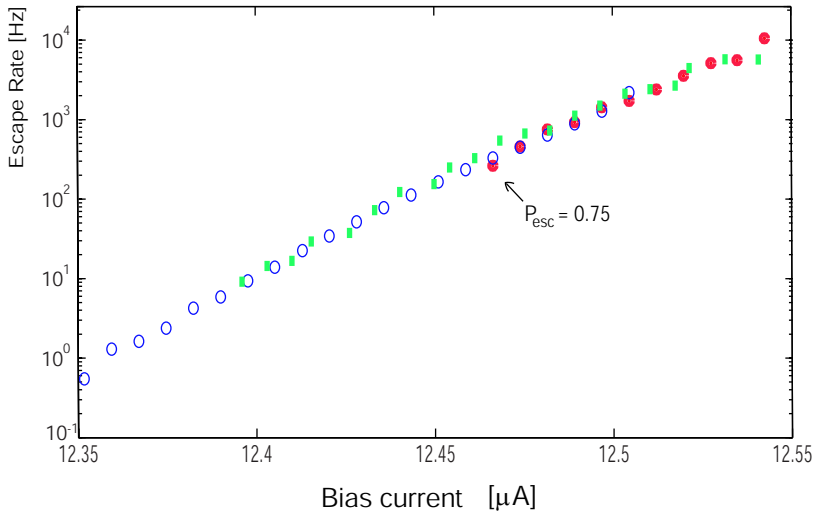

Figure 7: Comparison of the measured escape rates in a time-resolved setup. Blue circles and red points belong to the same procedure of data acquisition, but the method of data evaluation uses an exponential fit of the escape probability histogram for red points, where the blue points are obtained by solving Eq. (1) for Γ. The green rectangles are obtained by our previous approach, which results in the same values for the escape rate but costs much more measurement time.

to the long rise time, the phase will most probably escape already before the target value of current is reached. We could extend this upper limit of the escape rate to about 3 kHz by replacing the RC filters in the current lines by filters with a higher cut-off frequency of 50 kHz. The RC rise time of the bias current leads, measured by applying a current pulse to the junction biased in its resistive state, is found to be 24 μs.

A large range of measurable escape rates is especially important when scanning a bias current range and searching for the resonance between an externally applied microwave and the junction's energy levels. At a resonance, two levels are coupled by the microwave and transitions between them occur by absorption and stimulated emission of photons, leading to an enhancement in the escape rate from the excited level. The spectroscopic width of this enhancement relative to its center frequency gives a measure for the quality factor, which reflects the energy relaxation rate in the qubit.

Using the same setup used for time-resolved measurements, we can now observe the exponential decay from the excited state. The major difference is that we trigger the microwave source to generate a microwave pulse shortly after setting the constant level of the bias current. The data is evaluated in the same way as for the determination of the ground-state escape rate, except that we regard only events which occur when the microwave is switched on. Escape rates from the first excited state of up to 1 MHz could be readily measured. Fig. 8 shows a result of this technique.

Coherent dynamics. Under the resonant microwave drive, the excited level population will oscillate at the Rabi frequency as long as the system remains coherent. Due to decoherence, the population is expected to decay with a characteristic time which is for our sample approximately $\tau = Q \,/\, \omega_{01} \approx 12$ ns. Observation of coherent Rabi oscillations is our primary goal. It will allow us to directly measure the decoherence times of the qubit.

We searched for signatures of coherent oscillations by doing a Fourier analysis of the time-resolved escape probability, limiting ourselves to a short time interval after the onset of the microwave. Alternatively, to increase the time-resolution, we used a DC readout pulse

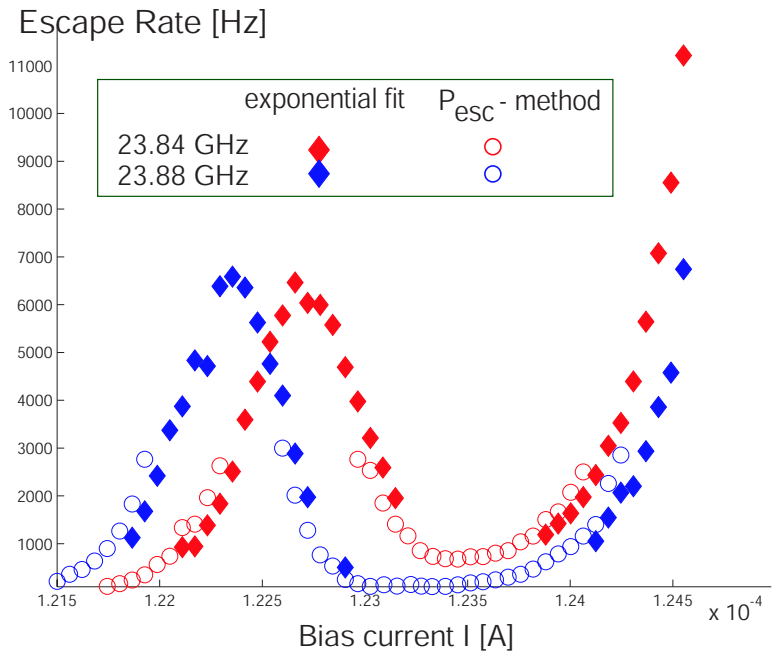

Figure 8: The escape rate of a junction irradiated by 23.84 GHz (red symbols) and 23.88 GHz (blue symbols) shows resonance peaks at specific bias currents. Circles are obtained using the new method of estimating the escape probability. Our previous evaluation approach (diamonds) limits gaugeable escape rates to above 1 kHz.

of sub-nanosecond duration. This pulse increases the tunnelling rates from all levels. Due to the shorter lifetime of the excited state, this pulse results either in immediate or delayed tunnelling, depending on whether the qubit is in its excited or ground state, respectively. To this date, we did not succeed to observe Rabi oscillations in our junctions.

1.4 Conclusion and outlook

Although we do now possess the necessary tools to observe coherent quantum dynamics of the qubit, we could not yet achieve to do so in experiment. The major reason is that the intrinsic quality factor of the qubits, when investigated with our current setup, is too low. The coherence time is expected to be lowered by the qubit design: although the junction can be shielded from the biasing wires through filters and impedance mismatches, the degree of decoupling from the environment must be made larger. One possibility is to use an on-chip superconducting coil, which will produce a screening current from an applied constant magnetic field, and connect this coil to the junction. We are currently doing experiments with new samples where the junction will not any longer be biased through directly connected wires, but through this kind of superconducting broadband impedance transformer. Doing so, we expect to increase the impedance of the environment seen by the junction by three orders of magnitude as compared to the stripline filter approach. Another source of decoherence in the investigated qubit type was found to be the switching to the voltage state, in which the junction is heated and quasiparticles, i.e. normal electrons, are generated. We come to this conclusion as we found that the time which is necessary to cool down the junction after each measurement is of several milliseconds. This drawback is also solved when the junction is embedded in a superconducting loop, because the voltage will be kept close to zero nearly all time.

2 Testing of multi-Josephson junction persistent supercurrent qubits

2.1 Introduction

A geometric approach for quantum computation using non-Abelian holonomic gate operators has been recently proposed by Phachos et al [6]. Duan et al [7] have proposed an implementation of non-Abelian holonomic quantum computation using trapped ions. Alternative system, where geometric quantum computation can be implemented, is based on multi-Josephson junction qubit of a discretized and flattened version of the triangular long Josephson junction (JJ) prism discussed in Refs. [8, 9].

One of its flat versions is shown in Fig. 9. Potential energy profile of this qubit is periodic and each period has two minima. These minima of the potential profile of this system are

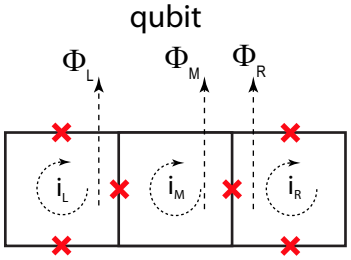

Figure 9: 2D version of Yukon's qubit.

associated with the circulating current in the left ($i_L = I_{\min}$, $i_R = 0$) and right loops ($i_L = 0$, $i_R = I_{\min}$). The fluxes Φ_M and $\Phi_L + \Phi_R$ determine the barrier height. The barrier height depends on the width of the wells, the width of the barrier and of the barrier and $I_{\min}$. By changing the differential flux ($\Phi_L - \Phi_R$) between the left and right loops one can make the potential profile asymmetric. Since the qubit potential well and qubits interaction with external flux are defined by non-Abelian holonomy or Berry phase, the basis for both qubit and gate properties can be said to be of geometric origin.

The standard qubit based on the single-loop SQUID has a double well potential at half frustration and relies on the external field. The important feature of the Yukon's qubit is that it should be less sensitive to fluctuations of the external magnetic field. Another interesting property of this qubit is that the barrier height can be changed without changing the symmetry of the potential profile. The main difference between multi-qubit circuit based on the Yukon's qubits and single-loop qubits is that former ones can be coupled by Cirac-Zoller type of bus [10].

2.2 Design

We have designed the circuit shown schematically in Fig. 10. The design rules set several constrictions for the parameters of the qubit and dc-SQUID. In the theoretical calculations the qubit cell inductance is neglected. However, technological processes put the lower limit on the size of cell. The cells of the qubit was of minimum allowed size, 5x5 μm. The estimated inductance of the cell is about 3 pH. We have made several samples with different junction sizes (red crosses in Fig. 10): 3x3 μm^2, 4x4 μm^2 and 5x5 μm^2.

For detecting signal from qubit we have used a two hole dc-SQUID. In order to have an overdamped junctions (green crosses in Fig. 10), they were shunted by a resistance of 10 Ω. The size of each cell of the SQUID was made 70x60 μm^2. The SQUID cells were coupled to the input coils of 11 turns each. The input coils are turned in opposite directions. They

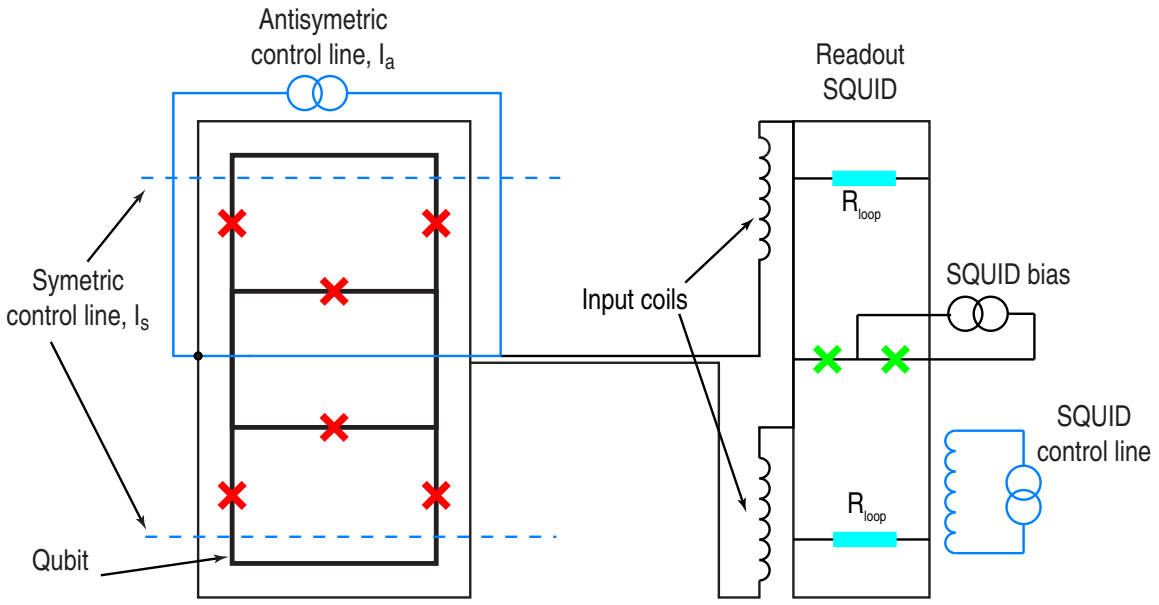

Figure 10: Designed qubit with dc-SQUID readout

are connected to the parallel loop gradiometer, which is coupled to the qubit. In order to filter noise at rf range, both cells of the SQUID were shunted with resistor of 12 Ω (in Fig. 10 marked as $R_{\rm loop}$). A magnetic flux through the SQUID cell is controlled by a current through the SQUID's control line and the qubit state is controlled by currents through symmetric and antisymmetric control.

Technological process allowed only two metallic layers. In order to have qubit and gradiometer on top of each other we had to connect them galvanically. SQUID and input coils are also connected with each other.

2.3 Experiments

Samples according to our design were prepared at the foundry of IPHT Jena (Germany). The critical current density was about 240 A/cm^2 at 4.2 K. Due to shunting resistors the SQUID's junctions were overdamped at 4.2 K. As a working point of the read-out SQUID we have chosen the bias current and frustration with largest dV/dI and dV/df_{SQ} response amplitudes. We have fixed the current I_s through symmetric control lines while sweeping the current I_a of antisymmetric control line and measuring the voltage of the SQUID. The experimental results presented here are taken from two identically designed circuits on the same chip, so all their parameters are almost identical.

In Fig. 11(a) we present voltage-field curves of the sample "Jena-SQUID-2" with the qubit junction size 3x3 μm^2. The black line corresponds to increase of the current and the red one to decrease of the antisymmetric current I_a for $I_s = 300\,\mu$A through each of the symmetric control lines.

The hysteresis shown in Fig. 11(a) starts at $I_a = 2.7$ mA and vanishes at $I_a = 2.95$ mA (hysteresis size $\delta I_a = 250\,\mu$A). The effective change of the frustration through SQUID for the hysteresis signal is about Δf$\simeq$3.0 $\times 10^{-2}$. This signal is about twice as large as the signal in our previous experiments reported in Ref. [11].

Fig. 11(b) the read-out SQUID response for the circuit "Jena-SQUID-1" is shown. This sample also has the same junction size as the circuit "Jena-SQUID-2", 3x3 μm^2. The current through symmetric control lines is $I_s = 290\,\mu$A. The size of the hysteresis is $\delta I_a = 405\,\mu$A. The

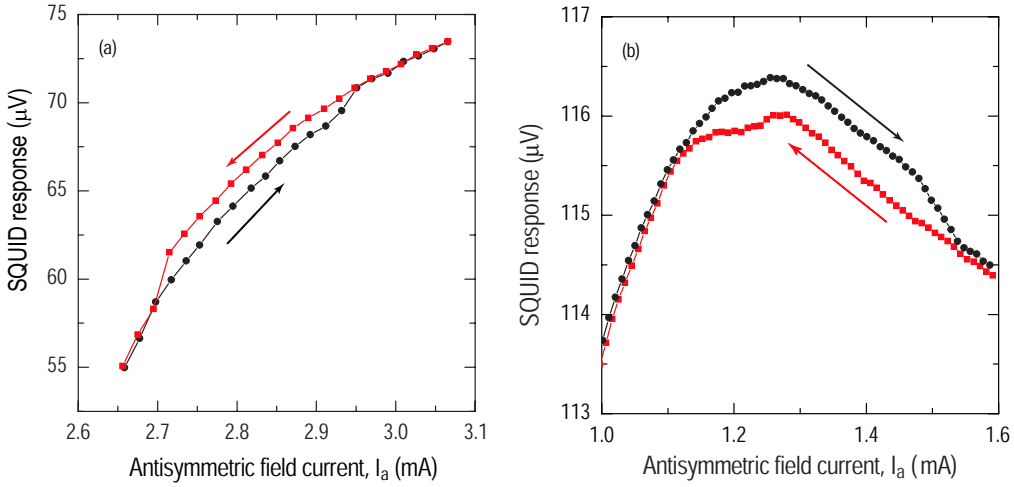

Figure 11: Read-out SQUID response to increase (black line) and decrease (red line) of current I_a for sample "Jena-SQUID-2" (a) and for sample "Jena-SQUID-1" (b).

largest effective change of the frustration through SQUID loop is about $\Delta f \simeq 3.0 \times 10^{-3}$, ten times smaller than for the sample "Jena-SQUID-2". For this sample switching between two different states is smooth, which means that we may not fully exclude some flux movement in the films. The same signal, however, can be observed after temperature recycling.

Despite of the identical parameters of the qubit junctions the two circuits show hysteresis at different magnitude of the antisymmetric field and the hysteresis size is different.

We repeated the above described measurements for different currents through symmetric control lines. The hysteresis range in antisymmetric field does not depend on the current through the symmetric control lines, while its position shifts towards larger values of antisymmetric field.

Measurements with qubits with larger junction size, samples Jena-SQUID-5 (junction size 4x4 μm^2) and Jena-SQUID-7 (junction size 4x4 μm^2), have shown no hysteretic behavior of the read-out SQUID signal.

3 Measurements of radiation from series-parallel arrays

3.1 Background

Mixed series-parallel Josephson junction arrays (SPA) have been proposed by Jain et al [12] for high-frequency oscillators. Shitov suggested [13] a modification of that scheme using microwave matching of the dc bias leads and array cells. A sketch of such an array consisting of only 5 junctions is shown in Fig.12.

The main idea of this layout is that Josephson junctions (indicated by crosses in Fig. 12) are arranged in parallel for a DC current I_B applied to the array as shown in the figure, while the AC voltages generated by the junctions add up in series. The interference between the junctions can be tuned by an externally applied magnetic flux through the cells. At half frustration, the amplitude of AC oscillations as well as the radiation power will reach a maximum. The DC component of the voltage across the dipole antenna, which is attached to the edge junctions of the array, should be equal to zero for an even number of junctions, but should be determined by a single junction voltage for odd number of junctions. The

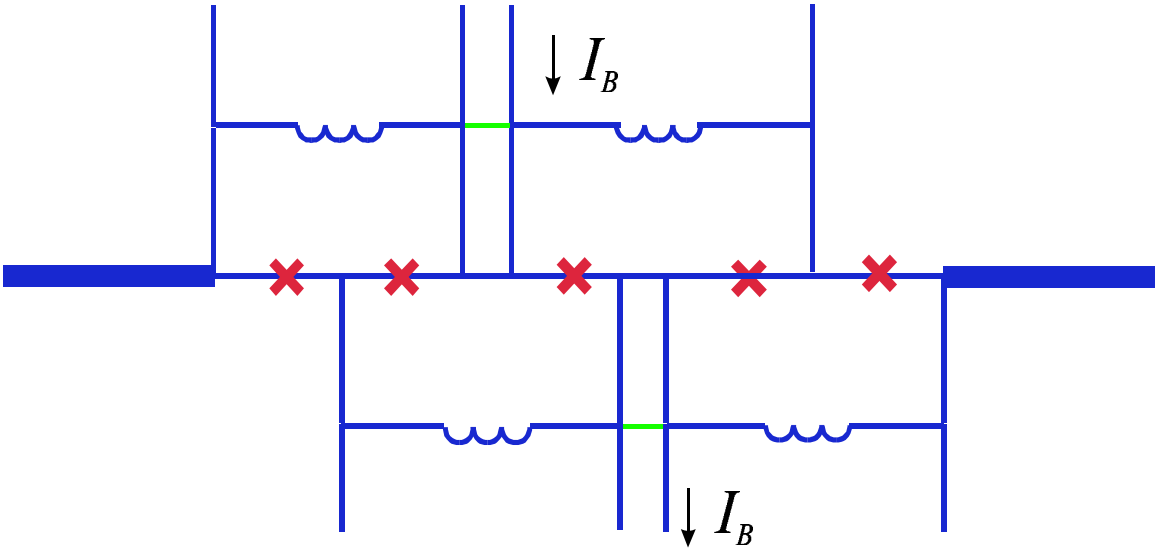

Figure 12: Series-parallel Josephson junction array scheme

amplitude of the AC voltage is expected to increase with the number of junctions. The array has to be operated in a resonant mode which frequency is determined by the cell inductance and junction capacitance.

In our previous measurements with SPA [15], the resonance frequency was too low to measure radiation from resonant steps with our heterodyne receiver. Here, we report measurements on redesigned arrays. The main improvement in the design is that we decreased the loop inductance. From calculations, we expected the main resonance to be found at about 100 GHz.

3.2 Measurements and discussion

The samples according to our layout were fabricated at Hypres foundry. The cell size of the prepared arrays is about $5 \times 20\,\mu\text{m}^2$, the size of each junction is $3 \times 3\,\mu\text{m}^2$. The arrays with a total of 22 junctions have been measured in helium vapor at a temperature of about 7.6 K. We estimated the temperature from the gap voltage, which was 1.5 mV. The critical current density at the measurement temperature was determined to be about 200 A/cm^2. In order to change the frustration through the array cell, an external magnetic field perpendicular to the arrays plane was applied.

The measured array has shown three pronounced steps at voltages of about 100 μV, 180 μV and 350 μV. In Figs. 13(a), 14(a) and 15(a) the field-voltage dependencies for all three steps are presented by open circles. These steps appear at different frustrations. We were able to measure radiation from all of them.

The I-V curve of the array at frustration of about 0.61 is shown in Fig. 13(b) by red symbols. There are two steps at voltages near 100 μV and 150 μV. Our receiver was tuned to the center frequency of 92 GHz. We have measured the radiation from the lower step (100 μV), which means that the detected power is the second harmonic of the Josephson frequency. The black lines corresponds to the measured power. This curve has two peaks around the lower step on the current-voltage characteristic. These two peaks correspond to an increasing and decreasing bias current. The measured power from the lowest step vs. frustration is shown in Fig. 13(b) (red symbols). The largest power detected from the lowest step was about 2pW. Radiation from this lowest step was measured at frustrations about 0.25 and 0.75.

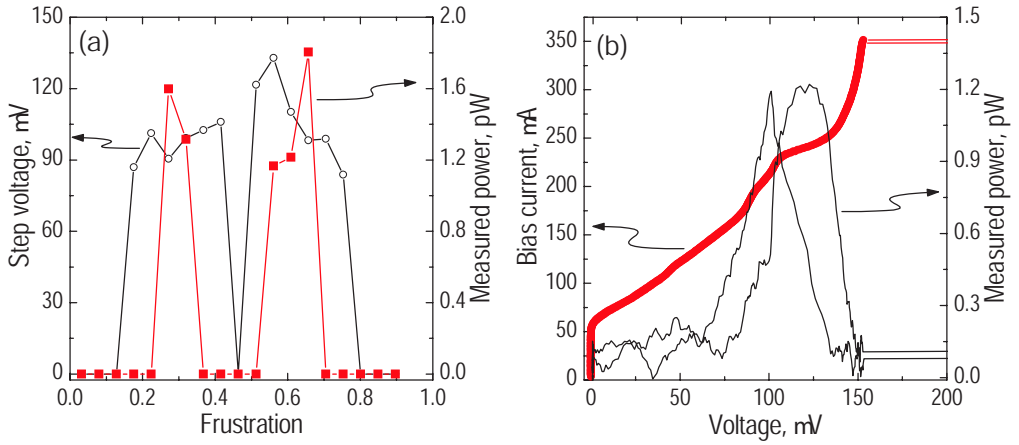

Figure 13: (a) Frustration dependence of the lowest step voltage (open circles) and measured power (red symbols), (b) I-V curves (red symbols) and measured power (line) at frustration 0.61.

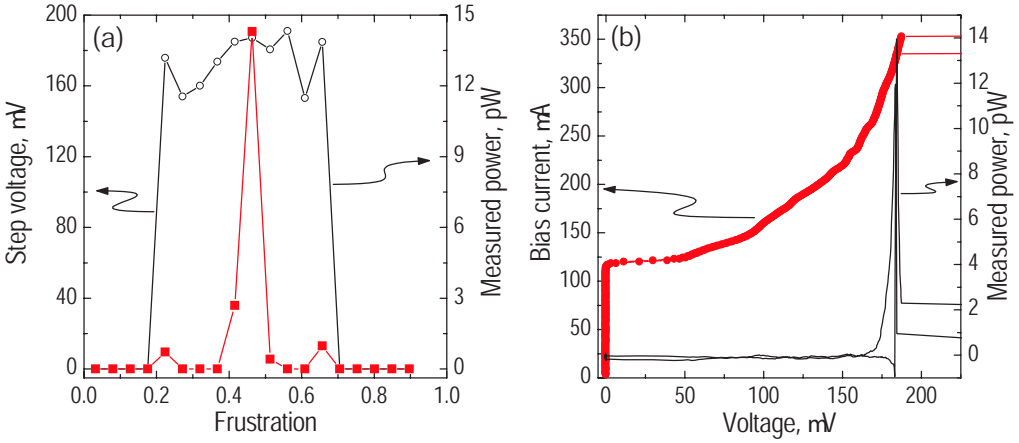

Figure 14: (a) Frustration dependence of the middle step voltage (open circles) and measured power (red symbols), (b) I-V curves (red symbols) and measured power (line) at frustration 0.46.

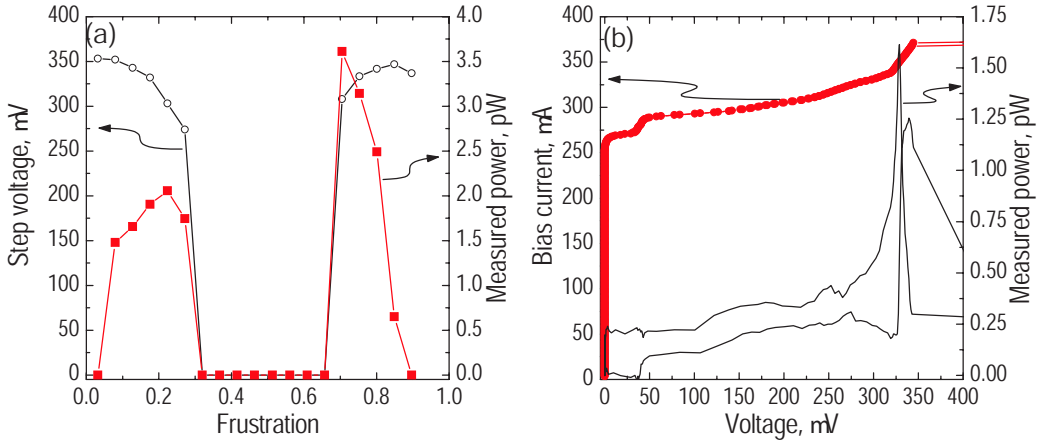

Figure 15: (a) Frustration dependence of the highest step voltage (open circles) and measured power (red symbols), (b) I-V curves (red symbols) and measured power (line) at frustration 0.13.

The I-V curve of the array at frustration of about 0.46 is shown in Fig. 14(b) by red symbols. The resonant step appears at voltages of about 184 μV. The power curve (black line) has two peaks at voltages of about 184 μV, which corresponds to 89 GHz. The peaks are very close to each other and almost overlap. These two peaks correspond to increasing and decreasing bias current. The measured power from the middle step vs. frustration is shown in Fig. 13(b) (red symbols). Radiation from this step was observed mainly at half frustration. The detected radiation power at this frustration was about 14 pW.

The I-V curve of the array at frustration of about 0.13 is shown in Fig. 15(b) by red symbols. At this frustration the array has its resonance at a voltage of about 350 μV. At this frustration also the power curve (black line) has two peaks at voltages of about the step voltage, which corresponds to 170 GHz. This frequency is about two times larger then the detection frequency, i.e. here we detect radiation of the second subharmonic of the Josephson frequency. The measured power from this step vs. frustration is shown in Fig. 13(b). The largest radiation power detected from this highest step was about 3.6 pW. Radiation from this step was detected at frustrations $0.1 - 0.3$ and $0.7 - 0.85$.

4 Summary

We investigated prototypes of quantum bits based on current-biased Josephson junctions. Decoherence is the major obstacle against quantum computation using this type of qubit. We evaluated our idea of reducing decoherence by embedding the junction in a microwave-engineered filter circuit. Although the characteristics of the fabricated circuits meet the designed specifications, the amount of decoherence could not be reduced by the microwave filter. In contrast, decoherence could be successfully suppressed by reducing the amount of low-frequency current noise to the junction. The coherence time could so be extended by a factor of five by fabricating current-dividers in the bias circuitry. Unforeseen complications in the operation of the designed microwave circuits, like flux trapping, turned out to be the major drawback of this approach.

The development and test applications of new experimental techniques to manipulate and read-out the quantum state of the qubit directly in the time-domain were successful. Our approach to state readout using a dc-pulse of nanosecond width was implemented and works. With a new evaluation method, we could extend the range of experimentally accessible

lifetimes and at the same time reduce the necessary data acquisition time.

Despite these achievements, coherent oscillations of the quantum bit dynamics could not be observed by us up to date. The rather short coherence time of ≈ 10 ns, which is typical for the qubits, is due to the direct connection of the junction to the room temperature electronics and current noise reaching the junction in this way. Currently, we are investigating samples which are galvanically decoupled from the environment by means of superconducting transformer circuits which are expected to overcome the major obstacle of large decoherence.

We reported our measurement of a flatted JJ prism qubit. We have observed that qubits with junction size 3x3 μm^2 show the readout response has a hysteretic behavior. However, for qubits with larger junction size the read-out response does not show any hysteresis. The experimental results show that for both samples the hysteresis size does not depend on the current through symmetric control lines, which is rather puzzling for the moment.

The reported successful measurements on a series-parallel array show three main resonant steps at voltages 100 μV, 180 μV and 350 μV. We have been able to measure radiation from all three steps at different frustration. The largest detected radiation power was about 14 pW from the first harmonic of the Josephson frequency of the step at voltages near 184 μV. For the other two steps the measured radiation power was few pW and corresponds to the second harmonic (100 μV step) and second subharmonic (350 μV step) of the Josephson frequency.

References

[1] J. M. Martinis, S. Nam, and J. Aumentado, Rabi oscillations in a large Josephson-junction qubit, *Phys. Rev. Lett.* **89**, 117901 (2002)

[2] A. Wallraff, A. Lukashenko, C. Coqui, A. Kemp, T. Duty and A. V. Ustinov, Switching current measurements of large area Josephson tunnel junctions, *Rev. Sci. Instr.* **74** (8), 3740 (2003)

[3] David P. DiVincenzo, The physical implementation of quantum computing, *Fortschritte der Physik* **48**, 771 (2000)

[4] The microwave design of this circuit was performed in collaboration with S. Shitov.

[5] S. Kleff, S. Kehrein, and J. von Delft, Exploiting environmental resonances to enhance qubit quality factors, *cond-mat*/0304177 (2003)

[6] J. Pachos, P. Zanardi and M. Rasetti, Phys. Rev. A **61**, 010305 (2000)

[7] L-M. Duan, J.I. Cirac and P. Zoller, Science, **292**, 1695 (2001)

[8] S.P. Yukon, Physica C **368**, 320 (2002)

[9] S. P. Yukon, Proceedings of MQC2, 2002, Naples, Italy.

[10] J.I. Cirac, and P. Zoller, Phys. Rev. Lett. **74**, 4091 (1995)

[11] A. A. Abdumalikov, and A. V. Ustinov, Interim Report No. 4, *Experiments on coupled Josephson junctions devices*, contract F61775-01-WE045, February 2003.

[12] A.K. Jain, K.K. Likharev, J.E. Lukens and J.E. Sauvageau, Phys. Rep. **109**, 309 (2000).

[13] S. Shitov, private communication (2000).

[14] A. A. Abdumalikov and A. V. Ustinov, Final Report, *Testing of Josephson array antennas and trim currents tunning*, contract F61775-00-C0004, September 2001.

[15] A. A. Abdumalikov and A. V. Ustinov, Interim Report No. 3, *Experiments on coupled Josephson junctions devices*, contract F61775-01-W-E045, August 2002.

5 Declarations, disclaimers, and acknowledgment

This material is based upon work supported by the EOARD under Contract No. FA8655-03-1-3037.

The Contractor, Prof. Dr. Alexey Ustinov, hereby declares that, to the best of its knowledge and belief, the technical data delivered herewith under Contract No. FA8655-03-1-3037 is complete, accurate, and complies with all requirements of the contract.

1) Acknowledgement of Sponsorship: Effort sponsored by the Air Force Office of Scientific Research, Air Force Material Command, USAF, under grant number FA8655-03-1-3037. The U.S. Government is authorized to reproduce and distribute reprints for Government purpose notwithstanding any copyright notation thereon.

2) Disclaimer: The views and conclusions contained herein are those of the author is and should be interpreted as necessarily representing the official policies or endorsements, either expressed or implied, of the Air Force Office of Scientific Research or the U.S. Government.

3) Disclosure of inventions: I certify that there were no subject inventions to declare during the performance of this grant.

DATE: August 3, 2004

Name and Title of Authorized Official:

Alexey Ustinov, PhD
Professor of Experimental Physics
University of Erlangen-Nuremberg, Germany